Experimental Measurement and CFD Model Development of Thick Wind Turbine Airfoils with Leading Edge Erosion

David C. Maniaci[1], Edward B. White[2], Benjamin Wilcox[2], Christopher M. Langel[3], C.P. van Dam[3], Joshua A. Paquette[1]

[1]Sandia National Laboratories, Albuquerque, NM 87185
[2]Texas A&M University, College Station, TX 77843
[3]University of California, Davis, Davis, CA 95616
Corresponding author: dcmania@sandia.gov

Abstract. Leading edge erosion and roughness accumulation is an issue observed with great variability by wind plant operators, but with little understanding of the effect on wind turbine performance. In wind tunnels, airfoil models are typically tested with standard grit roughness and trip tape to simulate the effects of roughness and erosion observed in field operation, but there is a lack of established relation between field measurements and wind tunnel test conditions. A research collaboration between lab, academic, and industry partners has sought to establish a method to estimate the effect of erosion in wind turbine blades that correlates to roughness and erosion measured in the field. Measurements of roughness and erosion were taken off of operational utility wind turbine blades using a profilometer. The field measurements were statistically reproduced in the wind tunnel on representative tip and mid-span airfoils. Simultaneously, a computational model was developed and calibrated to capture the effect of roughness and erosion on airfoil transition and performance characteristics. The results indicate that the effects of field roughness fall between clean airfoil performance and the effects of transition tape. Severe leading edge erosion can cause detrimental performance effects beyond standard roughness. The results also indicate that a heavily eroded wind turbine blade can reduce annual energy production by over 5% for a utility scale wind turbine.

1. Introduction

Leading edge erosion is an emerging issue in wind turbine blade reliability, causing performance decreases and additional maintenance costs. Through the U.S. DOE Blade Reliability Collaborative, researchers from Sandia National Laboratories (SNL), Texas A&M, and U.C. Davis have recently addressed the subject of performance loss. The surface roughness caused by blade leading edge erosion was characterized in the field and used to inform wind tunnel tests. Researchers then used the wind tunnel measurements to develop a predictive model of roughness-induced boundary layer transition for wind energy applications. A further analysis calculated the effects of erosion on wind turbine energy capture [1-6].

This first phase of measurement and modeling focused on an airfoil that is typically used on the tip region of a utility-scale wind turbine blade, the NACA 63_3-418, which has a maximum thickness to chord ratio of 18%. The aerodynamic characteristics of the thicker airfoils located at the inboard region of a wind turbine blade are significantly different than the characteristics of thinner, outboard airfoils. There is a lack of critical experimental data of the effect of roughness and erosion on thicker airfoils, and collection of such data is needed to calibrate the model for application to the inboard region of a blade. A second phase of this research is underway to measure the aerodynamic

Content from this work may be used under the terms of the Creative Commons Attribution 3.0 licence. Any further distribution of this work must maintain attribution to the author(s) and the title of the work, journal citation and DOI.
Published under licence by IOP Publishing Ltd

performance of an airfoil section model in a wind tunnel at conditions simulating those encountered by the inboard region of a wind turbine blade. The SERI S814 airfoil, which has a maximum thickness to chord ratio of 24%, was selected for this purpose due to it having desirable characteristics for code validation, as well as the availability of previously published transition data. The model was constructed using an innovative multi-part process, which will enhance the ability to locate transition using infrared thermography.

2. Experimental Method and Preliminary Results

The NACA 63_3-418 airfoil was used as the baseline configuration in the Oran W. Nicks Low Speed Wind Tunnel at Texas A&M University. The wind-tunnel model is 0.813 m in chord and 2.1 m in span. The model was mounted vertically in the 2.1-m-high, 3.05-m-wide wind tunnel test section, resulting in 4.9% blockage. Pitch variations were provided by the floor turntable. Approximately 12 mm of clearance exists between the model end plates and ceiling and floor. To provide various erosion configurations, the model was designed with a removable leading edge at 15% chord. Two piano hinges along the upper and lower main body are used to securely attach the leading edge. The hinge pins can be removed through holes in the wind tunnel floor, allowing simple model changes while creating a consistent interface between the leading edge and airfoil main body. Model pressure ports were placed near center span to avoid wall interference near stall. Interference between ports is avoided by offsetting each pressure port 9.5 mm in the spanwise direction.

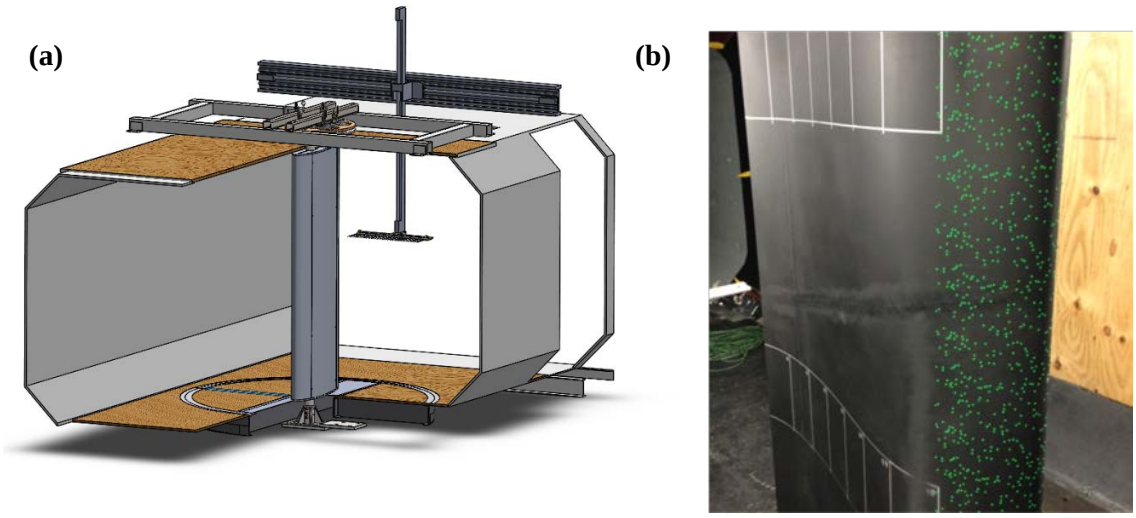

Figure 1: (a) Section view of wind tunnel test section with installed model and wake-rake and **(b)** model with leading-edge roughness applied

Typical roughness patterns including insect carcasses, paint chips, and erosion were characterized in field measurements then manufactured using vinyl stickers and a 3D-printed leading edge [2, 4, 7]. Roughness extent for the insect carcasses was calculated using a simulation code, which estimates the expected insect impingement locations [8]. Sparsely distributed roughness was tested at three heights and five surface-area-coverage densities, extending from 4.5% chord on the upper surface to 12.5% chord on the lower surface of the NACA 63_3-418 and 4.5% chord on the upper surface to 19.2% on the lower surface of the NREL S814. Erosion on the 63_3-418 was simulated using the 3D-printed leading edge that duplicates a field-measured erosion pattern [7]. Reynolds numbers during the test was varied between 0.8×10^6 and 4.8×10^6.

Lift and pitching moment were calculated by integrating the surface pressure distribution. Because static pressure is not measured at the trailing edge, a weighted average was calculated from the nearest two ports at 92% and 95% chord. Drag was calculated using a wake integral. A wake rake was placed 0.9c downstream of the wing trailing edge. The wake rake has 25 pitot probes and three static probes.

At higher angles of attack when the flow has separated, a large unsteady region results in poor data quality. Therefore, drag results at high angles of attack are suspect. For the current study, this region is of no interest.

Results indicate minimal effect from paint-chip roughness. Figure 2 reveals that, as distributed roughness height and density increase, the lift-curve slope, maximum lift coefficient, and lift-to-drag ratio all decrease. Roughness height was found to be more important in determining performance than roughness density. A 60˚ zigzag trip-strip was also tested with a 6 mm wavelength, 9 mm peak-to-peak amplitude, and a nominal height of 500 µm. The trip-strip was placed at 2% chord (x/c) on the upper surface and 5% chord on the lower surface. Clean and trip-strip configurations act as bounding cases for airfoil performance. For the 200 µm roughness configuration, stall is more gradual than in other roughness configurations, indicating possible changes in the separation mechanism for large roughness heights. At the lowest angles of attack, the drag coefficient of the 140 µm roughness diverges from the tripped and 200 µm cases toward the drag of the smaller roughness cases. These divergence points are also evident in other configurations and indicate a distinct change in the transition behavior at these angles.

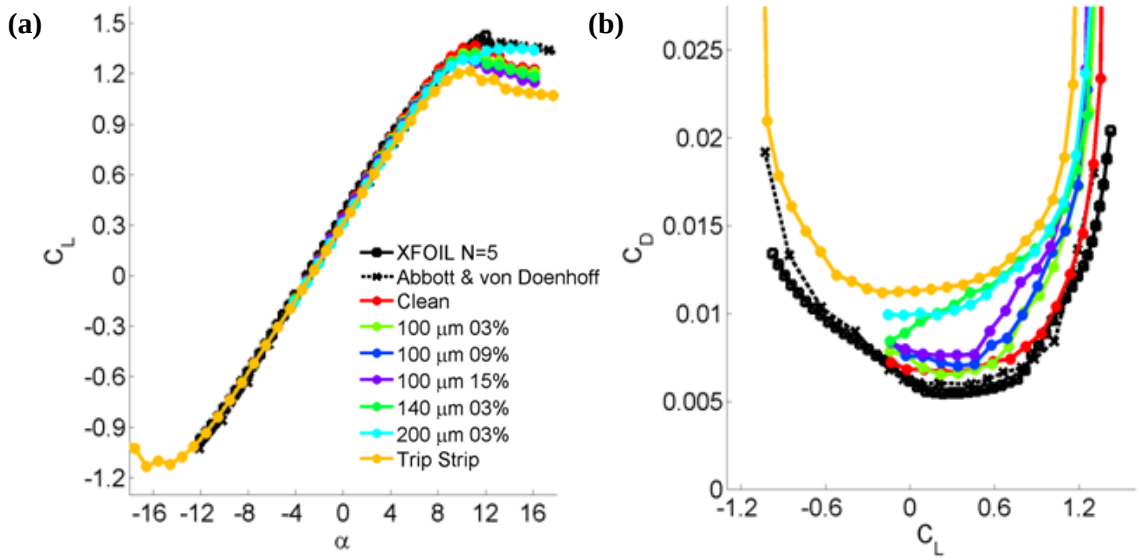

Figure 2: (a) Lift and **(b)** drag data for NACA 63_3-418 airfoil for various roughness conditions at Re = 3.2×10^6.

Laminar-to-turbulent transition was measured using infrared (IR) thermography. IR thermography leverages the difference in convection rates of laminar and turbulent flows and the temperature difference between the model and air to indicate transition location. Generally, the model surface temperature lags the ambient temperature variations as the tunnel heats up. The warmer, ambient air will heat a turbulent region faster than a laminar region. An IR image was acquired at each angle of attack or velocity during a test run. Images with a two dimensional transition front were analyzed by sight. Figure 3a shows an example IR image on the upper surface of the NACA 63_3-418 at 0° angle of attack and a chord-based Reynolds number of 3.2×10^6. As angle of attack or Reynolds number increases, natural transition triggered by Tollmien–Schlichting (TS) waves is replaced by roughness-induced bypass transition and the formation of turbulent wedges. Figure 3b shows the transition diagram corresponding to the same conditions as Figure 3a. The angle of attack at which bypass occurs is indicated with an arrow.

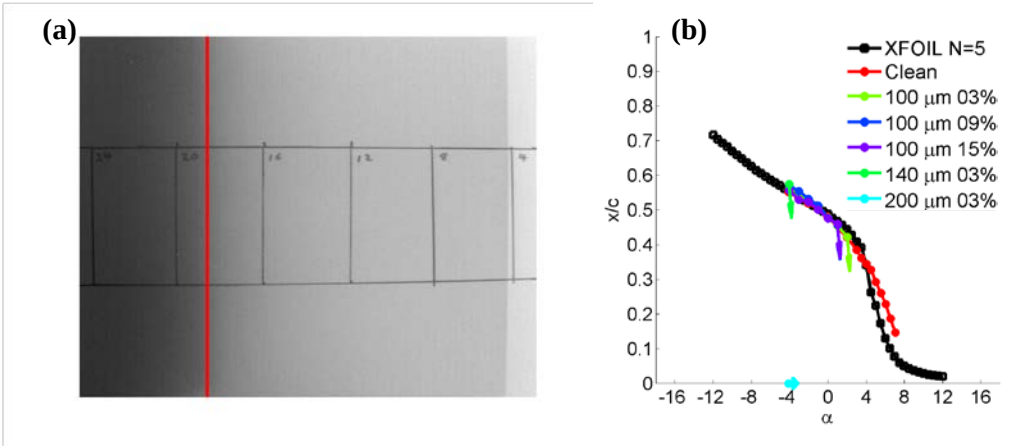

Figure 3: (a) IR thermography image showing TS-dominated transition at 0° angle of attack and **(b)** transition locations vs angle of attack for the NACA 63_3-418 at $Re_c = 3.2\times10^6$.

Measurements of the SERI S814 airfoil were also completed. The SERI S814 airfoil is a 24% thick airfoil which was developed specifically for the mid-span section of wind turbines. Wind tunnel tests of the NACA 63_3-418 airfoil guided the construction of the SERI S814 wind-tunnel model. Specifically, steps were taken so that the IR transition analysis that was performed on the upper surface of the NACA 63_3-418 could be repeated on both surfaces of the NREL S814. To accomplish this, the model was designed with all bolts internal to the model and a large region of constant thickness near the model's mid-span region which provides a section of constant thermal properties. Figure 4 compares the wind tunnel models for the two airfoils. The most distinct difference between the airfoil profiles is the increased thickness of the SERI S814 lower surface compared to that of the NACA 63_3-418.

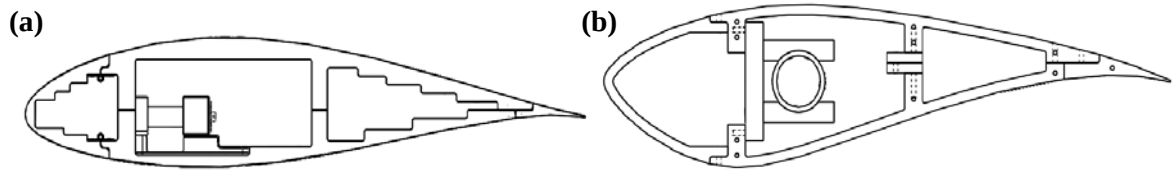

Figure 4: Comparison of **(a)** NACA 63_3-418 and **(b)** SERI S814 wind tunnel models.

The SERI S814 airfoil was tested using clean, trip-strip, and distributed roughness configurations at Reynolds numbers of 1.6×10^6, 2.4×10^6, 3.2×10^6, and 4.0×10^6. Three different roughness heights and three different roughness densities were tested for distributed roughness configurations. The same trip strip was used for the SERI S814 as that of the NACA 63_3-418 but was moved to 2% chord and 10% chord on the upper and lower surfaces, respectively, to match the trip strip locations used in similar tests by Somers [9]. Infrared analysis was not obtained for the lowest Reynolds number due to low temperature differences between the model and air. Lift and drag data was collected for all Reynolds numbers.

Variation in lift and drag data due to roughness for the SERI S814 is shown in Figure 5 and is similar to that of the NACA 63_3-418, with increased roughness height and density resulting in decreased lift-curve slope, maximum lift coefficient, and lift-to-drag ratio. At low angles-of-attack, roughness caused premature stall on the lower S814 surface which severely limits the lift and increases the drag for these angles-of-attack. The severe pressure-side stall was not evident on the NACA 63_3-418 airfoil and is likely due to the increased thickness of the SERI S814 airfoil. Comparisons of lift and drag data show that, in general, the SERI S814 airfoil exhibits larger losses in lift-curve slope, maximum lift, and lift-to-drag ratio than the NACA 63_3-418 airfoil. These results are compiled in Table 1.

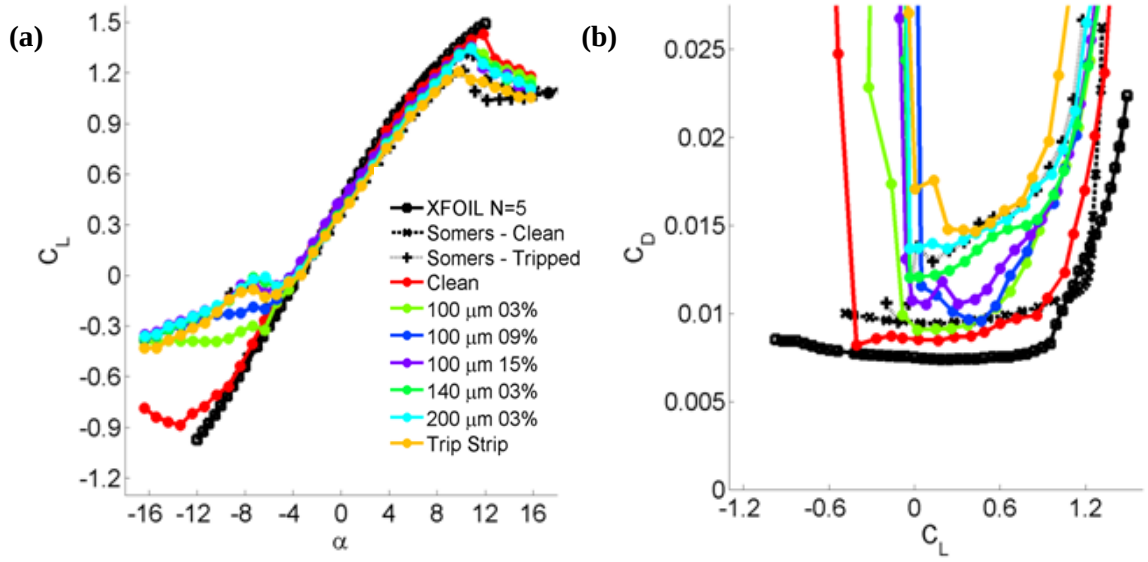

Figure 5: (a) Lift and **(b)** drag data for SERI S814 airfoil for various roughness conditions at Re = 3.2×10^6.

Table 1: Performance loss comparison for NACA 63_3-418 and SERI S814 airfoils for a variety of distributed roughness configurations at $Re_c = 3.2\times10^6$.

Configuration	$dc_L/d\alpha$		$c_{L,max}$		$(c_L/c_d)_{max}$	
	NACA 63_3-418	SERI S814	NACA 63_3-418	SERI S814	NACA 63_3-418	SERI S814
Clean	6.86 rad^{-1}	6.32 rad^{-1}	1.37	1.44	106	88
100 μm 03%	-0.7%	-7.2%	-3.2%	-5.9%	-17.8%	-30.3%
100 μm 09%	-3.0%	-8.6%	-4.4%	-6.5%	-23.0%	-31.4%
100 μm 15%	-4.5%	-11.2%	-6.2%	-5.3%	-31.1%	-32.4%
140 μm 03%	-3.3%	-6.2%	-3.9%	-6.1%	-35.0%	-33.2%
200 μm 03%	-4.1%	-5.3%	-1.5%	-6.5%	-36.6%	-38.0%
Trip Strip	-6.2%	-9.7%	-11.0%	-16.2%	-41.2%	-45.5%

Upper-surface transition data for the SERI S814 in Figure 6a shows that the TS-dominated transition front moves forward as angle-of-attack is increased at a fixed Reynolds number. Bypass transition (indicated with an arrow) occurs at the lowest angles-of-attack for the largest roughness height. Bypass angles of attack increase for increasing roughness height and density. Lower-surface transition data given in Figure 6b shows bypass occurring at the highest angles-of-attack for the largest roughness heights and moving to lower angles-of-attack as height is decreased. The TS-dominated transition front on the lower surface stays very near the point of maximum thickness for all angles-of-attack due to the large adverse pressure-gradient which destabilizes the flow past this point.

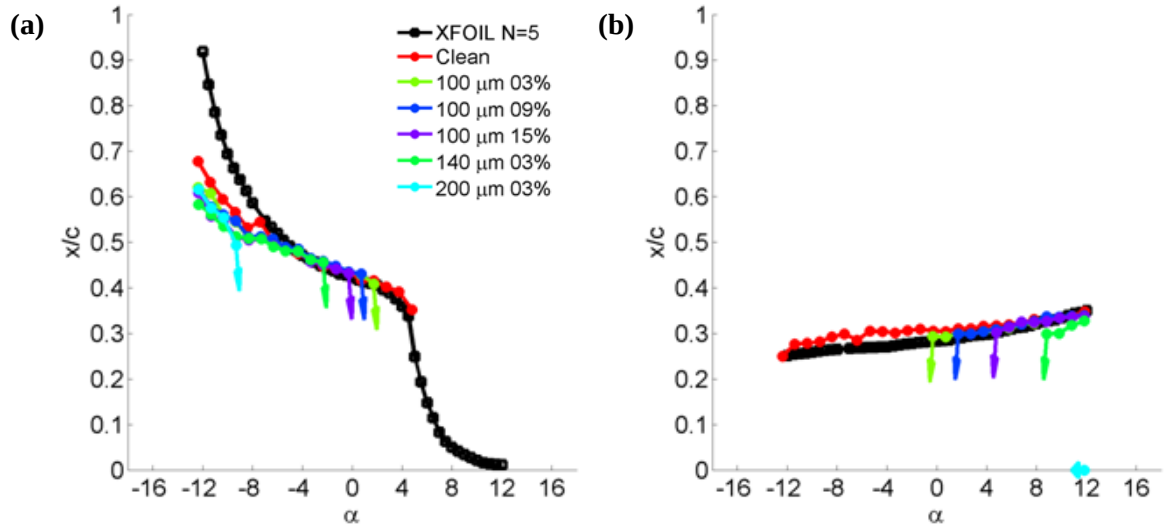

Figure 6: Transition locations for **(a)** upper and **(b)** lower surfaces of SERI S814 airfoil for various roughness conditions at $Re_c = 3.2\times10^6$.

Tani defines a roughness Reynolds number $Re_k = u_k k/\nu$ where k is the roughness height, ν is the dynamic viscosity, and u_k is the velocity at the roughness height for the corresponding undisturbed (no-roughness) boundary layer [10]. He also defined a critical roughness Reynolds number as the roughness Reynolds number where bypass transition occurs and found that this critical value is dependent upon the ratio of roughness height to diameter for cylindrical roughness. Critical roughness-based Reynolds numbers for both airfoils were computed by combining the experimental bypass angles-of-attack with boundary layer data from the CFD model (discussed in later sections). Table 2 shows that, with the exception of the 100 μm configurations on the NACA 63_3-418, all computed critical roughness Reynolds numbers fall within the expected range offered by Tani's correlation.

Table 2 : Critical roughness Reynolds numbers for each airfoil at $Re_c = 3.2\times10^6$.

Configuration	$Re_{k,crit}$ – experimental NACA 63_3-418	$Re_{k,crit}$ – experimental NREL S814		$Re_{k,crit}$ - theoretical range (Tani correlation)
	Upper Surface	Upper Surface	Lower Surface	
100 μm 03%	318	214	206	168-252
100 μm 09%	270	201	194	168-252
100 μm 15%	254	189	175	168-252
140 μm 03%	240	266	238	193-289
200 μm 03%	227	226	-	222-333

3. Model Development and Calibration

Presently and in the past, most roughness models are fundamentally correlation based due to the physical complexities of the disturbances introduced by surface roughness. Carrying on with this type of strategy, the present work seeks to model the macroscopic effects of roughness on flow characteristics. There have been a number of different studies on how roughness affects the turbulent boundary layer [11]; however, the first order effect of premature laminar-turbulent transition has yet to be extensively modeled. The formulation takes advantage of a recently developed local correlation transition model to include transition effects in the roughness model predictions. The transition model

includes two additional transport equations that represent the empirically correlated transition criteria, and a scaling parameter to simulate the transition process [12]. An important consideration is the form of the equations allows integrated effects to be incorporated in the model. Roughness is modeled by introducing an additional scalar quantity that is produced at rough wall boundaries and distributed using an additional transport equation. This quantity is then used to modify the correlated transition criteria. The input to the model is a scalar equivalent sand grain roughness height, ks.

The calibration of the model first involved establishing a formulation that could account for as many relevant flow variables as possible, while maintaining a high level of generality. In addition to the equivalent sand grain roughness height, the model contains a dependence on the local pressure gradient and wall shear stress. One of the ongoing challenges is parameterizing the roughness distributions into a suitable k_s that can be used in the roughness model formulation. The calibration of the model was performed under some assumptions regarding the nature of this k_s parameter. Primarily, given a fixed roughness distribution, there is a one-to-one mapping between different heights of the roughness elements (k) and an equivalent sand grain roughness height, k_s. This allowed the functional relationship between k_s and the roughness model variable to be established by isolating the changes in the flow behavior to changes in the height of the roughness used. Changes in distribution density are then accounted for by scaling the k_s parameter. The experimental results for the NACA 63_3-418 from the first phase of the research effort were used to begin the calibration of the model. The highest density (15%) was initially chosen due to the projected similarity to a "sand grain" roughness and availability of data. The k_s input into the model was then the non-dimensional roughness height (k/c) at 15% density. More information regarding the model formulation can be found in [3, 5].

The procedure involved first examining all the cases together and adjusting model parameters to correct areas where the model was clearly producing global discrepancies. As the model began producing more accurate results a more formal process was developed to examine each case to try and identify the required integrated change in transition criteria for the model to produce the experimental result. As the objective was to identify an integrated effect, an optimization across all the experimental cases was possible to try and construct functions that would best match all the integrated quantities.

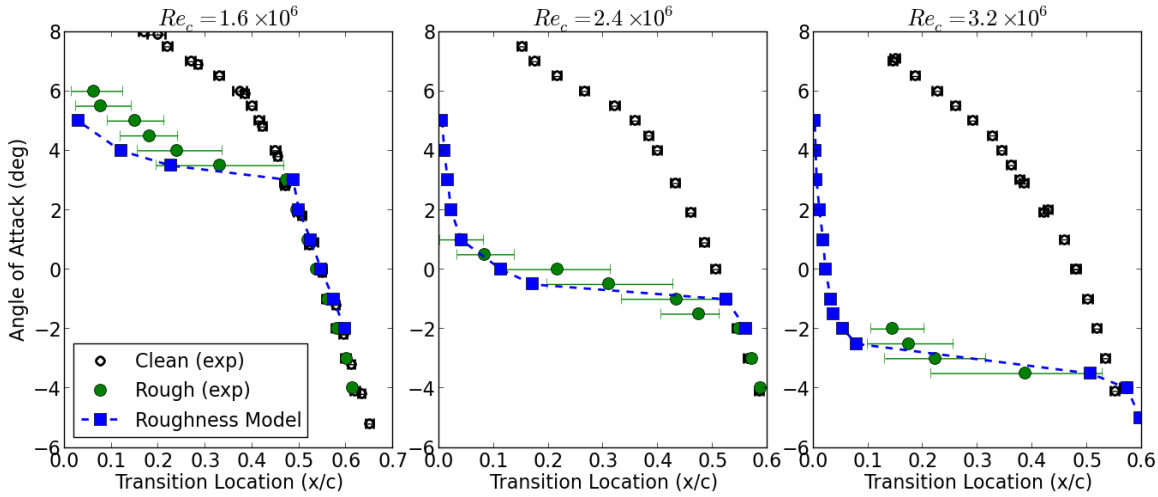

Figure 7: Transition locations for upper surface of the NACA 63_3-418 airfoil for clean and rough configurations at various Reynolds numbers, roughness height 140 μm (k/c = 172 × 10^{-6}) at 15% density roughness applied, k_s = 172 × 10^{-6} input into roughness model.

The predicted transition locations in Figure 7 demonstrate very favorable agreement with the experimental results. Many of the main characteristics, such as the angle of attack where the transition location begins to move forward rapidly are predicted correctly at all Reynolds numbers. Figure 8 shows the predicted drag polars for the same configurations.

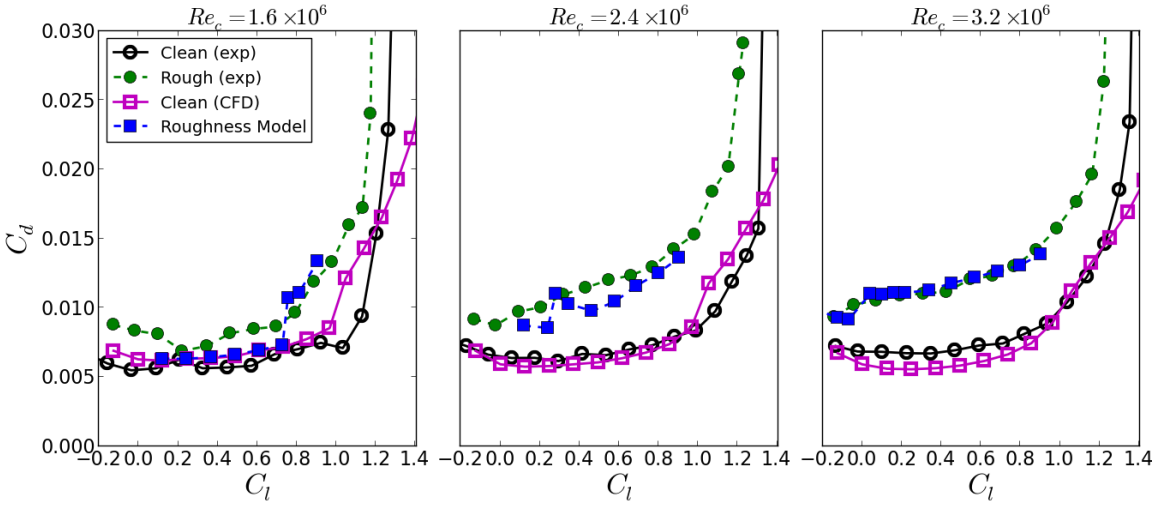

Figure 8: Drag polars for the NACA 633-418 airfoil for clean and rough configurations at various Reynolds numbers, roughness height 140 **μ**m (k/c = 172 × 10-6) at 15% density roughness applied, ks = 172 × 10-6 input into roughness model.

4. Model Validation

After the second phase of the experimental campaign, the model calibrated to the NACA 63_3-418 data was applied to SERI S814 airfoil and compared to the experimental results. The results shown in Figures 9 and 10 show the predicted upper surface transition location and drag polars.

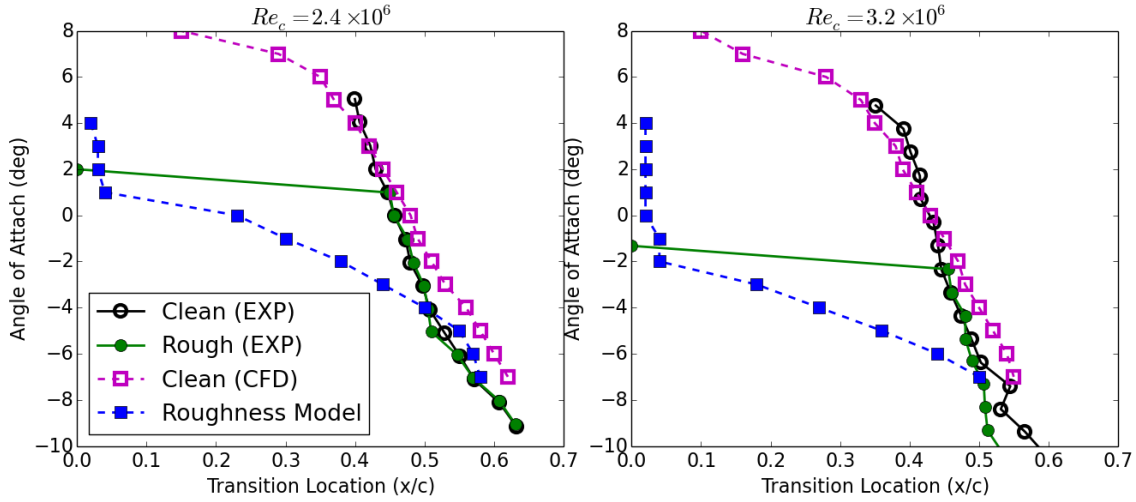

Figure 9: Transition locations for upper surface of the SERI S814 airfoil for clean and rough configurations at various Reynolds numbers, roughness height 140 **μ**m (k/c = 172 × 10^{-6}) at 03% density roughness applied, k_s = 172 × 10^{-6} input into roughness model.

On the whole the model tends to predict a more gradual movement of the transition location. This implies the influence of the pressure gradient function in the model needs to be adjusted slightly to accurately represent the bypass transition observed. However, once the bypass angle has been reached the model predicts transition effectively at the leading edge. It should also be noted that the roughness

distribution density of the experimental results shown here are lower compared to the NACA 63_3-418. Moving forward some adjustment will be made of the k_s parameter input into the roughness model. A slight reduction should help with the experimental agreement and be consistent with the reduced distribution density.

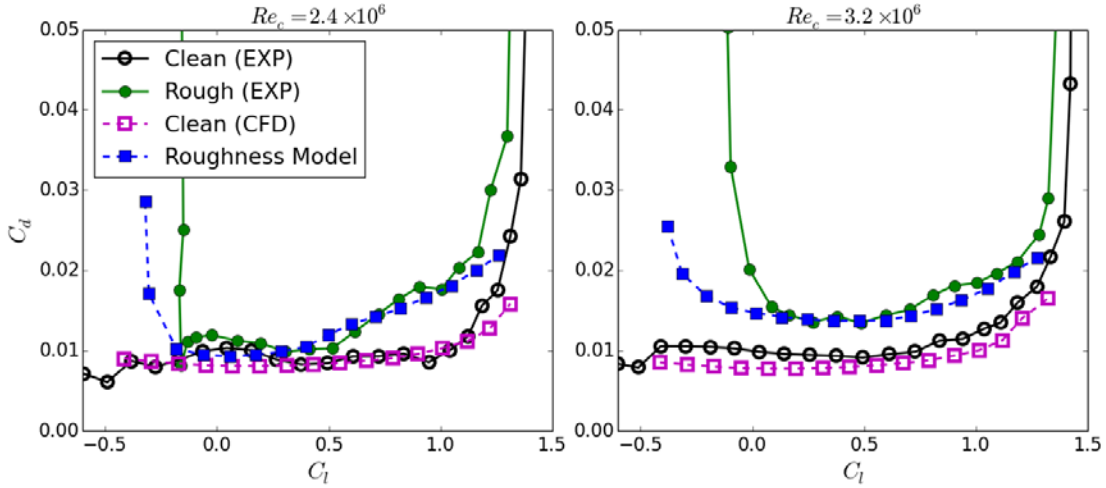

Figure 10: Drag polars for the SERI S814 airfoil for clean and rough configurations at various Reynolds numbers, roughness height 140 μm (k/c = 172 × 10^{-6}) at 03% density roughness applied, k_s = 172 × 10^{-6} input into roughness model.

A favourable characteristic of the model is the ability to predict the drag spike at low angles of attack caused by stalling on the lower surface. There is some delay in this rise at Re = 3.2×10^6 but the model does a very good job of predicting drag in the linear regime of the lift curve.

The results of the roughness model applied to the SERI S814 have demonstrated both the reliability of the formulation, and areas in which it can be improved. Notably, the influence of pressure gradient needs to be increased to adequately represent the rapid shift in transition location as observed on the SERI S814. Using the new data collected and the results from the NACA 63_3-418, the model is currently undergoing another calibration iteration. More details regarding this procedure and the full model formulation will be published in the future.

5. Conclusion

The leading edge erosion research project at Sandia National Laboratories has occurred over several phases, involving multiple organizations. The first phase of work involved measurements of blade surface roughness and erosion at an operational utility wind farm using a profilometer. The field measurements were statistically reproduced in wind tunnel tests on representative tip and mid-span airfoils with publically available data, respectively the NACA 63_3-418 and SERI S814.

The variation in lift and drag data due to roughness for the SERI S814 is similar to that of the NACA 63_3-418, with increased roughness height and density resulting in decreased lift-curve slope, maximum lift coefficient, and lift-to-drag ratio. Comparison of lift and drag data shows that, in general, the SERI S814 airfoil exhibits larger losses in lift-curve slope, maximum lift, and lift-to-drag ratio than the NACA 63_3-418 airfoil, which is likely due to the increased thickness to chord ratio of the S814.

The experimental results indicate that the effects of field roughness fall between clean airfoil performance and the effects of transition tape. Severe leading edge erosion can cause detrimental performance effects beyond standard roughness. The results also indicate that a heavily eroded wind turbine blade can reduce annual energy production by over 5% for a utility scale wind turbine [4].

A computational model was developed to capture the effect of roughness and erosion on airfoil transition and performance characteristics. The model formulation takes advantage of a local correlation transition model to include transition effects in the roughness model predictions. The

model includes an explicit dependence on roughness height, local pressure gradient, and wall shear stress, with an initial calibration performed for these parameters based on the NACA 63_3-418 from the first phase of the research effort. In the second phase of the research, the model results were compared to the experimental results of the S814 airfoil, which established the reliability of the model as well as areas of potential improvement.

Future work includes further model development, as well as publicly releasing the experimental data through the DOE Atmosphere to electron (A2e) Data Archive and Portal.

6. References

[1] Ehrmann R S, White E B, Maniaci D C, Chow R, Langel C M and van Dam C P 2013 Realistic leading-edge roughness effects on airfoil performance *31st AIAA Applied Aerodynamics Conf.* (American Institute of Aeronautics and Astronautics) AIAA-2013-2800

[2] Ehrmann R S and White E B 2014 Influence of 2D steps and distributed roughness on transition on a NACA 63(3)-418 *32nd ASME Wind Energy Symp.*(American Institute of Aeronautics and Astronautics) AIAA-2014-0170

[3] Langel C M, Chow R, van Dam C P, Rumsey M A, Maniaci D C, Ehrmann R S and White E B 2014 A computational approach to simulating the effects of realistic surface roughness on boundary layer transition *52nd Aerospace Sciences Meeting* (American Institute of Aeronautics and Astronautics) AIAA-2014-0234

[4] Langel C M, Chow R, Hurley O F, van Dam C P, Maniaci D C, Ehrmann R S and White E B 2015 Analysis of the impact of leading edge surface degradation on wind turbine performance. *33rd Wind Energy Symp.* (American Institute of Aeronautics and Astronautics) AIAA2015-0489

[5] Langel C M, Chow R and van Dam C P 2015 Further developments to a local correlation based roughness model for boundary layer transition prediction. *53rd AIAA Aerospace Sciences Meeting* (American Institute of Aeronautics and Astronautics) AIAA-2015-1232

[6] Langel C M, Chow R and van Dam C P 2016 A comparison of transition prediction methodologies applied to high Reynolds number external flows. *54th AIAA Aerospace Sciences Meeting* (American Institute of Aeronautics and Astronautics) AIAA-2016-0551

[7] Ehrmann, R S 2014 Degradation of Wind-Turbine Blade Performance due to Roughness Contamination (Ph.D. Dissertation, Texas A&M University)

[8] Wilcox B and White E 2015 Computational analysis of insect impingement patterns on wind turbine blades *Wind Energy* **19** 483-95

[9] Somers D and Tangler J 1996 Wind tunnel test of the S814 thick root airfoil *J. of Solar Energy Engineering* **118** 217-221.

[10] L Tani 1969 Boundary-layer transition *Annual Review of Fluid Mechanics* **1** 169-196

[11] Wilcox D C 1998 *Turbulence Modeling for CFD* ed 2nd (La Canada, California: DCW Ind.)

[12] Langtry R B and Menter F R 2009 A correlation-based transition model for unstructured parallelized computational fluid dynamics codes *AIAA J.* **47** 2894-906.

Acknowledgments

Matt Barone and Mark Rumsey of Sandia National Laboratories were instrumental in the initial phase of this work. This research was supported by the U.S. Department of Energy Office of Energy Efficiency and Renewable Energy Wind and Water Power Program.

Sandia National Laboratories is a multi-program laboratory managed and operated by Sandia Corporation, a wholly owned subsidiary of Lockheed Martin Corporation, for the U.S. Department of Energy's National Nuclear Security Administration under contract DE-AC04-94AL85000.